

# A rational design strategy for donors in organic solar cells: the conjugated planar molecules possessing anisotropic multibranches and intramolecular charge transfer†

Xue Yong and Jingping Zhang\*

Received 5th April 2011, Accepted 3rd May 2011

DOI: 10.1039/c1jm11423a

A strategy used to design novel high performance donor molecules for organic solar cells has been proposed by using double overlapping wave bands for broad and intensive absorption based on three types of high mobility building blocks, *i.e.*, the multibranching electron-rich fragment ( $D_F$ ), the different electron-excessive  $\pi$ -bridges ( $B_F$ ), and the proper electron-deficient fragment ( $A_F$ ). The multibranching  $\pi$ -conjugated  $D_F-(B_F)_n$  donor fragment provides the strong and broad short and middle wavelength  $\pi-\pi^*$  absorption, while the anisotropic multibranching intramolecular charge transfer between the  $D_F-(B_F)_n$  donor fragment and  $A_F$ s favours the strong and broad middle and long wavelength absorption. This concept is confirmed by the theoretical design of the planar X-shaped  $(A_F-B_F)_2-D_F-(B_F)_2-A_F)_2$  conjugated donor molecules constructed by benzo[1,2-*b*:4,5-*b'*]dithiophene as the  $D_F$ , bithiophene ( $B_F1$ ) and ethynyl-bithiophene ( $B_F2$ ) as anisotropic multiple  $B_F$ s, and cyano substituted thiazolo[3,4-*c*]pyridine as  $A_F$ s *versus* proper perylene diimide derivatives, as the acceptor material. Our theoretical results obtained with DFT and TD-DFT approaches for the electronic and spectroscopic properties, as well as the reorganization energies, reveal that the designed molecules are highly promising candidates towards high performance solar cell materials (*i.e.*, exhibiting a strong and broad spectroscopic absorption, high charge carrier mobility, and possessing a narrow energy gap as well as appropriate FMO energy levels *versus* specific acceptors).

## 1. Introduction

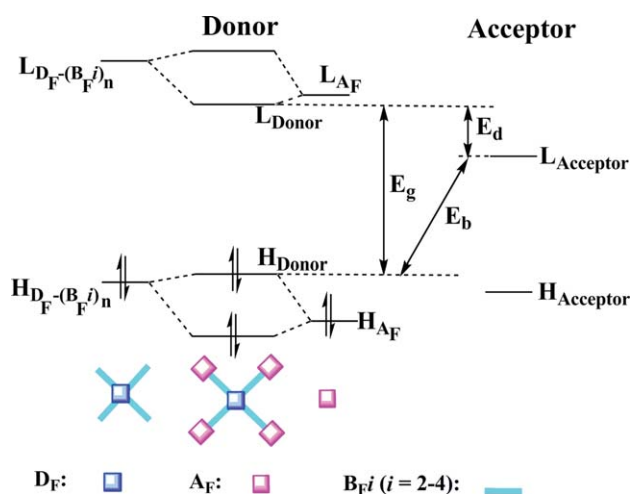
The interest in using small molecule semiconductors in organic solar cells based on a p-type semiconductor as a donor and an n-type semiconductor as an acceptor, has increased in recent years because of several key advantages, such as the monodispersity, and the ease of obtaining them in high purity, stability, and with reproducible properties.<sup>1,2</sup> The ideal donor should feature a low energy gap, strong and broad absorption covering the whole visible and near-infrared (NIR) region of the solar spectrum, high charge carrier mobility, and possess appropriate highest occupied molecular orbital (HOMO) and lowest unoccupied molecular orbital (LUMO) energy levels.<sup>3,4</sup>

Herein we propose a strategy to design novel donor molecules: using double overlapping wave bands for broad and intensive absorption in the visible and NIR region of solar spectrum based on three types of high mobility building blocks, *i.e.*, the multibranching electron-rich fragment<sup>5,6</sup> ( $D_F$ ), the different typical electron-excessive  $\pi$ -bridges<sup>7,8</sup> ( $B_F$ ), and the electron-deficient

fragment ( $A_F$ ).<sup>9,10</sup> The overlapping absorption spectrum of designed donor can be assigned by the  $\pi-\pi^*$  absorption band covering the short and middle (SM) wavelength region and push-pull anisotropic intramolecular charge transfer (ICT) absorption bands between  $D_F$ ,  $B_F$ , and  $A_F$  subunits covering the middle and long (ML) wavelength region. This can be achieved by judiciously constructing the anisotropic  $D_F-(B_F)_n-A_F$ , where  $i = 2-4$ ,  $n \geq 3$ , compounds with planar conformation (Scheme 1). The multibranching  $\pi$ -conjugated  $D_F-(B_F)_n$ , which is considered as the donor fragment in the molecule, provides the strong and broad absorption at the SM wave band, while the anisotropic multibranching ICT between the  $\pi$ -conjugated  $D_F-(B_F)_n$  donor fragment and the  $A_F$ s can exhibit strong and broad absorption<sup>11</sup> at the ML wave band. The consideration of this molecular design is due to the following reasons: (1) the use of a highly extended conjugated system<sup>12-14</sup> not only lowers the optical energy gap but also broadens the absorption spectrum; (2) the anisotropy of the multibranching ICT originating from the use of different  $B_F$ s might lead to an extension of the spectral response; (3) the electronic and optical properties of such compounds can be easily tuned by judiciously varying the  $D_F$ ,  $B_F$ , and/or  $A_F$ ; (4) the planarity of the conjugated compound is also important in obtaining a low energy gap<sup>4</sup> and enhancing the efficiency of the ICT; (5) the high charge transfer mobility of each building block

Faculty of Chemistry, Northeast Normal University, Changchun, 130024, China. E-mail: zhangjp162@nenu.edu.cn

† Electronic supplementary information (ESI) available: Computational, geometric and further details. See DOI: 10.1039/c1jm11423a



**Scheme 1** Schematic molecular design of the anisotropic  $D_F-(B_F^i-A_F)_n$ ,  $i = 2-4$ ,  $n \geq 3$ , compounds and orbital energy levels of the donor and acceptor material (L = LUMO, H = HOMO) in a organic solar cell.  $E_d$  is the energy difference between the LUMO of the donor and acceptor;  $E_g$  is the HOMO–LUMO energy gap of the donor molecule; and  $E_b$  determines the maximum open circuit voltage of the organic solar cell.

favors target compounds exhibiting better mobility. Additionally, the building blocks ( $D_F$ ,  $B_F$ , and  $A_F$ ) in the designed molecules contribute to the good geometrical-adjustment ability, which might favor the low reorganization energies corresponding to a higher charge mobility of target molecules.

The choice of appropriate building blocks is one of the key factors to design suitable molecules as donor materials. Generally, the following issues should be considered. (1) The  $D_F$  should possess multiple substitution sites, intensive absorption features, and good charge carrier mobility. The benzo[1,2-*b*:4,5-*b'*]dithiophene (BDT)<sup>5,6</sup> is a good candidate, where the fused benzene associated with the dithiophene rings provides the multiple- $\pi$ -conjugated branches. (2) Different electron-excessive  $\pi$ -conjugated chains (e.g., bithiophene and/or ethynyl-bithiophene) can be simultaneously used in a single molecule to serve as  $B_F$ s, which can act both as partial donor fragments in conjugation with  $D_F$  and the anisotropic routes for electronic transitions. Additionally, the introduction of a triple bond<sup>15</sup> might result in the red-shift of absorption bands and enhances the charge carrier mobility by providing planar conformation. (3) To enhance the  $D_F$ – $A_F$  interaction, lower the HOMO–LUMO energy gap (Scheme 1), and further strengthen and broaden the absorption, a strong  $A_F$  and short  $B_F$ <sup>8</sup> are preferred.

To test this strategy for the design of the donor materials, we present the theoretical design of molecules with an X-shaped  $(A_F-B_F)_2-D_F-(B_F^2-A_F)_2$  architecture, where the  $D_F$  is BDT,  $B_F1$  and  $B_F2$  are bithiophene and ethynyl-bithiophene, respectively, for the ease of synthesis. The proper  $A_F$ s for these molecules are selected as follows: first, we performed quantum calculations on isolated BDT,  $B_F1_2-D_F-B_F2_2$ , and six  $A_F$ s involving 1,3,5-triazine<sup>10</sup> and benzothiadiazole<sup>9</sup> (Fig. 1) to determine their orbital energy levels. Then, on the basis of these initial calculations of the individual fragments, suitable combinations of donor and acceptor moieties can be selected for the further design of organic donor candidates.

In addition, we selected various perylene diimide derivatives<sup>16–19</sup> (PDIs, see Scheme 2), as potential acceptors, *versus* the designed molecules as donors for the organic solar cell materials. Though computational results can provide insight for the material design, to the best of our knowledge, no theoretical work devoted to predicting the match between the donor and the acceptor materials has been reported so far. Herein, we also present an easy quantum chemical method to investigate the match between the designed donor and acceptor materials in terms of the HOMO and LUMO energy levels as a complementary approach for further experimental research.

## 2. Methodology

### 2.1. Computational details

The 6-31G(d) split valence polarized basis set was used throughout because it has been tested extensively and has been shown to yield reliable results for geometries and electronic properties of organic semiconducting materials.<sup>20–25</sup> The PBE1PBE<sup>26,27</sup> (also called PBE0) has been recognized to provide reliable predictions and interpretations of the molecular geometries, electronic properties, and optical properties of organic compounds bearing sulfur atoms.<sup>28–33</sup> To check the consistency of our calculation, preliminary density functional theory (DFT) and time-dependent density functional theory (TD-DFT) calculations were performed on BDT and the results were compared with available experimental data. Besides PBE0, the results of B3LYP<sup>34–36</sup> and B3P86<sup>37</sup> have also been compared with PBE0. According to our calculation, the most suitable method was found to be PBE0, which provided the accurate structure (the observed deviation from the X-ray data<sup>38</sup> is less than 0.031 Å in bond length and less than 1° in bond angles, Table S1†) and gave a reasonable estimate of the maximum absorption wavelength (349 vs. 347 nm,<sup>39</sup> Table S2†) compared with other methods.

The geometry optimizations were performed for the neutral, and ionic forms of the designed molecules at the PBE0/6-31G(d) level. No symmetry constraints were imposed during the geometry optimization. The isomers of the molecules under study were considered and the molecular geometries with the lowest energy were chosen. The ions were treated as open-shell systems using the unrestricted formalism (UPBE0/6-31G(d)). Following each optimization, the vibrational frequencies were obtained at the same level and the results showed that there was no imaginary frequency. On the basis of the optimized geometries, the electronic absorption spectra were systematically investigated by the TD-DFT method. The absorption spectra were simulated with a Gaussian-type curve and the full-width at half-maximum value used for the simulated spectra was 3000  $\text{cm}^{-1}$ . Although there are some limitations in the TD-DFT calculations, mainly due to approximations in the exchange correlation functional, the performances are reasonably good.<sup>40</sup> In combination with the preliminary results obtained with BDT, reliable results could be reasonably obtained for the designed molecules. Finally, reorganization energies of the two designed donors and the selected acceptors were obtained from the single point energies at the B3LYP/6-31G(d,p) level based on the PBE0/6-31G(d) optimized neutral, cationic and anionic geometries. All calculations were carried out with the aid of the Gaussian 09 program package.<sup>41</sup>

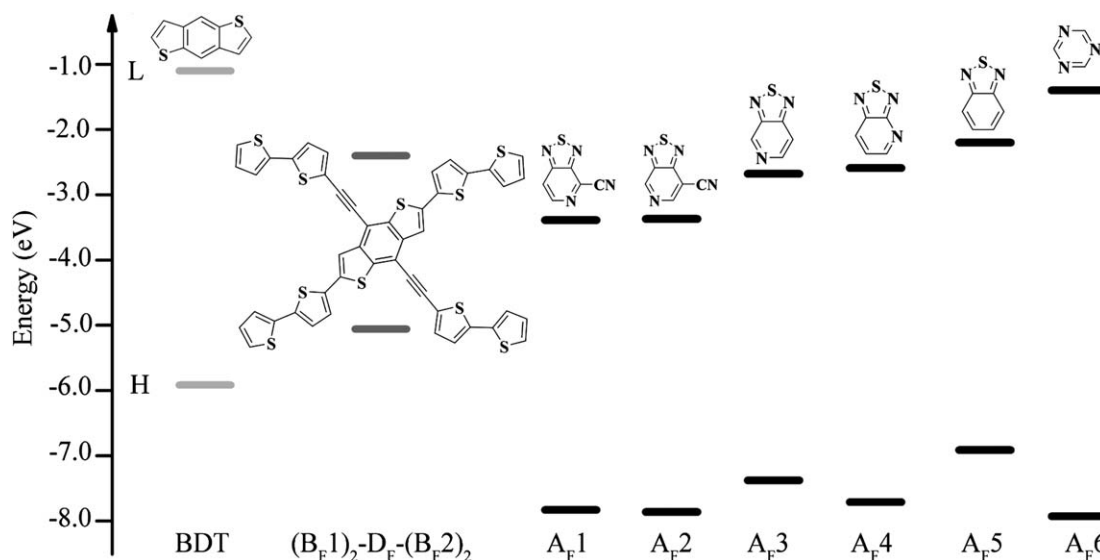
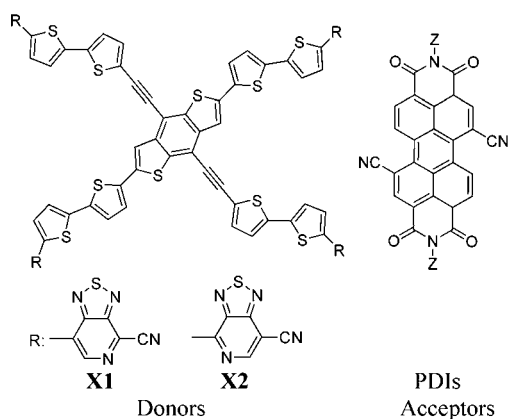


Fig. 1 Orbital energy levels of the HOMO and LUMO of BDT,  $\mathbf{B}_F\mathbf{1}_2\text{-D}_F\text{-B}_F\mathbf{2}_2$ , and the six  $\mathbf{A}_F\mathbf{s}$  (H = HOMO, L = LUMO).



Donors		PDIs Acceptors	
Molecules	Z-groups	Molecules	Z-groups
<b>PDI1</b>	$-(\text{CH}_2)_7\text{CH}_3$	<b>PDI6</b>	$-\text{CH}_2(\text{CH}_3)_2$
<b>PDI2</b>		<b>PDI7</b>	$-(\text{CH}_2)_3\text{CH}_3$
<b>PDI3</b>	$-\text{CH}_3$	<b>PDI8</b>	$-\text{C}(\text{CH}_3)_3$
<b>PDI4</b>	$-\text{CH}_2\text{CH}_3$	<b>PDI9</b>	$-\text{CH}(\text{n-C}_8\text{H}_{17})_2$
<b>PDI5</b>	$-(\text{CH}_2)_2\text{CH}_3$		

Scheme 2 Chemical structures of the two designed donors (**X1** and **X2**), and the acceptors (PDIs).

On the basis of the hopping model,<sup>42</sup> the charge transport mobility can be dominated by the reorganization energy, which is decomposed into internal (intramolecular) and external (intermolecular) contributions. The former corresponds to the geometry relaxation upon going from the neutral state geometry to the charged state geometry, and the latter arises from the changes in the electronic and nuclear surrounding medium upon charge transfer.<sup>43</sup> We considered only the intramolecular reorganization energy ( $\lambda$ ) here, as the nuclear polarization contributions are expected to be significantly smaller.<sup>43,44</sup> The respective intramolecular reorganization energy  $\lambda$  ( $\lambda_e/\lambda_h$  for electron/hole) could be obtained from an electronic structure as follows:<sup>45,46</sup>

$$\lambda_{\pm} = [E^{\pm}_0 - E_{\pm}] + [E^0_{\pm} - E_0]$$

Where, the  $E^{\pm}_0$  is the energy of the charged state corresponding to the neutral molecule. Similarly,  $E^0_{\pm}$  is the energy of the neutral state related to the optimized cationic/anionic structure.  $E_{\pm}$  and  $E_0$  are the energies of the optimized charged and neutral molecules, respectively.

## 2.2. The choice of electron-deficient fragments ( $\mathbf{A}_F\mathbf{s}$ )

As shown in Fig. 1 and Table S3†, we first investigated the HOMO and LUMO energy levels of the individual building blocks, *i.e.*, BDT,  $\mathbf{B}_F\mathbf{1}_2\text{-D}_F\text{-B}_F\mathbf{2}_2$ , and six  $\mathbf{A}_F\mathbf{s}$ , to screen the promising electron-donor fragment pairs for the design of the target donor materials for organic solar cells. As expected, the HOMO–LUMO energy gap decreases due to the introduction of four  $\mathbf{B}_F\mathbf{s}$  onto BDT, by extending the  $\pi$ -conjugation. At the same time,  $\mathbf{B}_F\mathbf{1}_2\text{-D}_F\text{-B}_F\mathbf{2}_2$  is confirmed as the donor fragment by its higher HOMO and LUMO energy levels compared to  $\mathbf{A}_F\mathbf{s}$ . On the other hand, the LUMOs of the six  $\mathbf{A}_F\mathbf{s}$  increase in the order of  $\mathbf{A}_F\mathbf{1}$ ,  $\mathbf{A}_F\mathbf{2} < \mathbf{A}_F\mathbf{3}$ ,  $\mathbf{A}_F\mathbf{4} < \mathbf{A}_F\mathbf{5} < \mathbf{A}_F\mathbf{6}$ , thereby, the electron-withdrawing strength decreases from  $\mathbf{A}_F\mathbf{1}$ ,  $\mathbf{A}_F\mathbf{2}$ ,  $\mathbf{A}_F\mathbf{3}$ ,  $\mathbf{A}_F\mathbf{4}$ ,  $\mathbf{A}_F\mathbf{5}$  to  $\mathbf{A}_F\mathbf{6}$ . These results indicate that the cyano (CN) substituent significantly enhances the electron-withdrawing ability of  $\mathbf{A}_F$ . Our calculated results are also in good agreement with a previous experimental study on the low-bandgap polymers,<sup>47</sup> whereby the benzene ring in benzothiadiazole substituted by a pyridine ring favors a stronger  $\mathbf{A}_F$ .

Although all six  $\mathbf{A}_F\mathbf{s}$  have lower HOMOs than  $\mathbf{B}_F\mathbf{1}_2\text{-D}_F\text{-B}_F\mathbf{2}_2$ , only  $\mathbf{A}_F\mathbf{1}$  and  $\mathbf{A}_F\mathbf{2}$  possess much lower LUMOs than  $\mathbf{B}_F\mathbf{1}_2\text{-D}_F\text{-B}_F\mathbf{2}_2$ , as shown in Fig. 1. Therefore, only the two stronger  $\mathbf{A}_F\mathbf{s}$  ( $\mathbf{A}_F\mathbf{1}$  and  $\mathbf{A}_F\mathbf{2}$ ) are ideal  $\mathbf{A}_F$  units for  $\mathbf{B}_F\mathbf{1}_2\text{-D}_F\text{-B}_F\mathbf{2}_2$  donor fragment to construct the candidates for donors in organic solar cells. Hence, two isomeric X-shaped  $(\mathbf{A}_F\text{-B}_F\mathbf{1})_2\text{-D}_F\text{-}(\mathbf{B}_F\mathbf{2}\text{-A}_F)_2$  conjugated molecules (abbreviated as **X1** and **X2**) were constructed (Scheme 2). For comparison, we also investigated  $\mathbf{B}_F\mathbf{1}_2\text{-D}_F\text{-B}_F\mathbf{2}_2$  and the related derivatives based on  $\mathbf{A}_F\mathbf{3}\text{--}6$ .

### 3. Results and discussion

The optimized structures for **X1**, **X2**, and **B<sub>F</sub>1<sub>2</sub>-D<sub>F</sub>-B<sub>F</sub>2<sub>2</sub>** are found to be planar conformations, as expected (Fig. 2 and Fig. S1†).

#### 3.1. Absorption properties

As expected, both **X1** and **X2** exhibit superior absorption properties when compared with the related derivatives based on **A<sub>F</sub>3-6** (Fig. S2a†). The excitation energies increase along with the decrease in the electron-withdrawing strength of the **A<sub>F</sub>s**. For example, the first excitation energies for **X1** and **X2** slightly increase from 1.67 to 1.71 eV (Table S4†). These low excitation energies confirm that two low energy gap conjugated molecules are successfully obtained by using the strategy proposed in this work. The absorption spectra of both **X1** and **X2** display two distinct intense and broad absorption bands at SM and ML wavelengths, respectively (Fig. 3). Such strong and broad absorption in the whole visible and NIR region of the solar spectrum is unusual for organic conjugated small molecules, which suggests that these two designed molecules are promising candidates for use as donors in organic solar cells. Inspection of the absorption spectra of **X1**, **X2**, and **B<sub>F</sub>1<sub>2</sub>-D<sub>F</sub>-B<sub>F</sub>2<sub>2</sub>** (Fig. S2b†) reveals that the introduction of **A<sub>F</sub>s** onto the **B<sub>F</sub>1<sub>2</sub>-D<sub>F</sub>-B<sub>F</sub>2<sub>2</sub>** donor fragment in **X1** or **X2** leads to an additional long wavelength absorption band. Furthermore, **B<sub>F</sub>1<sub>2</sub>-D<sub>F</sub>-B<sub>F</sub>2<sub>2</sub>** donor fragments may contribute to the SM wavelength absorption bands for both **X1** and **X2**; and the middle wavelength region might be ascribed to both the absorption of the **B<sub>F</sub>1<sub>2</sub>-D<sub>F</sub>-B<sub>F</sub>2<sub>2</sub>** donor fragment and partial ICT from **B<sub>F</sub>1<sub>2</sub>-D<sub>F</sub>-B<sub>F</sub>2<sub>2</sub>** donor fragment to **A<sub>F</sub>s**.

To elucidate the origin of spectra of **X1**, **X2**, and **B<sub>F</sub>1<sub>2</sub>-D<sub>F</sub>-B<sub>F</sub>2<sub>2</sub>**, the frontier molecular orbitals (FMOs) have been analyzed (Fig. 4-5 and Fig. S3†). The MOs of all the compounds have an overall  $\pi$  character. For each MO, the contributions from **B<sub>F</sub>1s** and **B<sub>F</sub>2s** are different, *e.g.*, the contribution from **B<sub>F</sub>2** to the LUMO of **X2** is 20%, while from **B<sub>F</sub>1** is 10% (Fig. 4 and Table S6†), which confirms that the use of different **B<sub>F</sub>s** provides anisotropic routes for electronic transitions. The calculated MOs

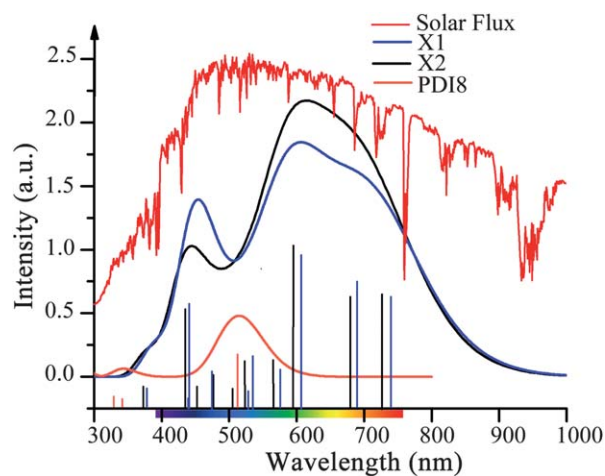


Fig. 3 Simulated absorption spectra of **X1**, **X2**, and **PDI8** at the TD-PBE0/6-31G(d) level compared with the Solar Flux for AM 1.5G.

distribution patterns of **X1** and **X2** are similar. The HOMOs, HOMO - 1s, HOMO - 2s, and HOMO - 3s are widely localized on the **B<sub>F</sub>1<sub>2</sub>-D<sub>F</sub>-B<sub>F</sub>2<sub>2</sub>** donor fragments. Furthermore, the HOMOs of **X1** and **X2** (-5.66 and -5.65 eV, see Table S7†) are close in energy. The LUMOs are distributed mainly over the **A<sub>F</sub>s**, with some contributions from **B<sub>F</sub>1s** and **B<sub>F</sub>2s**, while the LUMO + 1s are predominately located on the **A<sub>F</sub>s**. The LUMO + 2s basically contribute from **A<sub>F</sub>s** attached on the **B<sub>F</sub>2s** and the thiophene rings adjacent to them in **B<sub>F</sub>2s** with less contribution from **A<sub>F</sub>s** attached on the **B<sub>F</sub>1s**. While, the LUMO + 3s mainly focus on **A<sub>F</sub>s** attached on the **B<sub>F</sub>1s** and extend further on thiophene rings adjacent to them in **B<sub>F</sub>1s** with less distribution on **A<sub>F</sub>s** attached onto **B<sub>F</sub>2**. In the cases of LUMO + 4s and LUMO + 5s, the orbitals are strongly delocalized on the **B<sub>F</sub>1<sub>2</sub>-D<sub>F</sub>-B<sub>F</sub>2<sub>2</sub>** donor fragments with little involvement of the **A<sub>F</sub>s**. Interestingly, the careful inspection of Fig. S3† suggests that the HOMOs, HOMO - 1s, LUMO + 4s and LUMO + 5s for **X1** and **X2** mainly correspond to the HOMO - 1, HOMO, LUMO and LUMO + 1 of the **B<sub>F</sub>1<sub>2</sub>-D<sub>F</sub>-B<sub>F</sub>2<sub>2</sub>**, respectively. It is also worthy to highlight that the contributions from the **A<sub>F</sub>s** in the

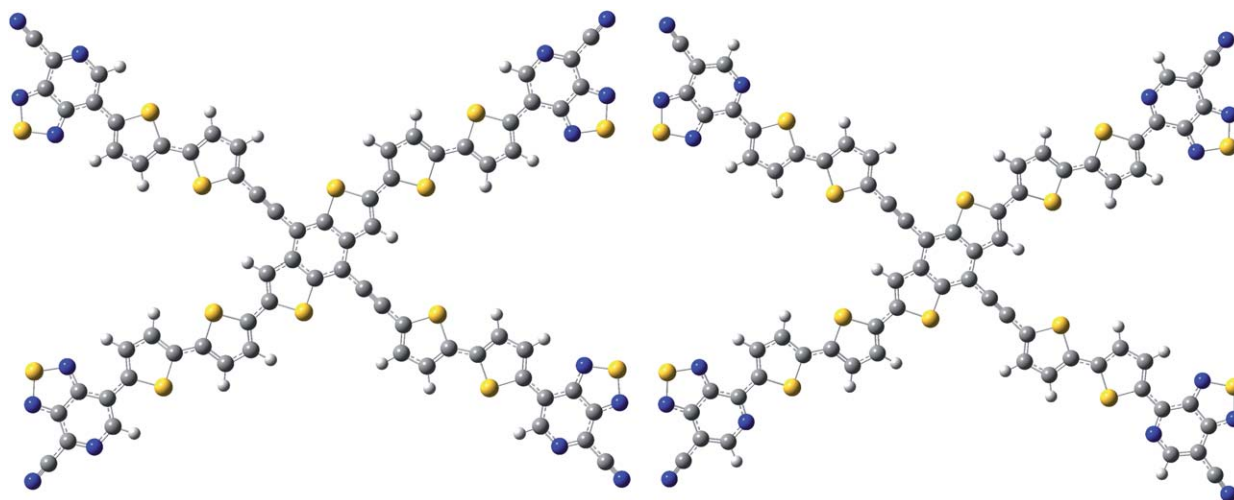


Fig. 2 The optimized structures of **X1** (left) and **X2** (right). (C, S, H, and N atoms are shown in gray, yellow, white, and blue, respectively).

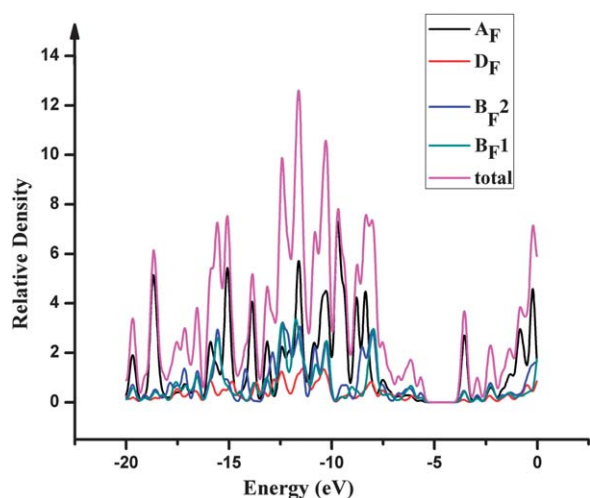


Fig. 4 Total and partial density of states around the HOMO and LUMO of **X2**.

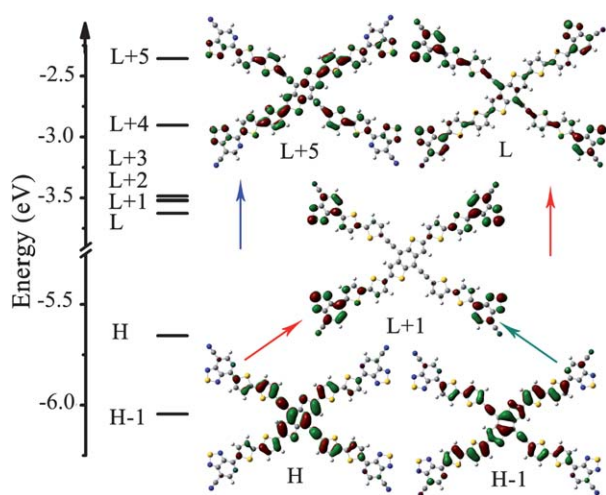


Fig. 5 Electron density plots of the FMOs of **X2** (H = HOMO, L = LUMO); arrows indicate main configuration of the main electronic excitations. The colour of the arrow represents the corresponding absorption region.

unoccupied molecular orbitals slightly decreases from **X1** to **X2** along with the slight decrease in the electron-withdrawing strength of the  $A_{F_S}$  (Table S6<sup>†</sup>). Consequently, the LUMO of **X2** ( $-3.63$  eV, see Table S7<sup>†</sup>) is slightly higher in energy than that of **X1** ( $-3.66$  eV, see Table S7<sup>†</sup>). **X1** therefore exhibits a slightly reduced HOMO–LUMO energy gap (2.00 vs. 2.02 eV for **X1** and **X2**, respectively, see Table S7<sup>†</sup>) which is in good accordance with their relative sequence of first excitation energies as discussed above, and a slight bathochromic in the maximum absorption of **X1** (732 nm, see Table S4<sup>†</sup>) with respect to **X2** (725 nm, see Table S4<sup>†</sup>).

To clarify the electronic transition nature for absorptions in different regions of the two designed molecules, the absorption spectrum of **X2** is analyzed as a representative in terms of the relevant absorption wavelength ( $\lambda_{ab}$ ), the main transition configurations as well as the oscillator strength ( $f$ ) (Table S4<sup>†</sup>). For **X2**, the ML region consists of four absorptions peaking at

725, 675, 598, and 562 nm, with  $f$  values of 1.142, 1.203, 2.052, and 0.496, respectively. This ML wavelength absorption band is assigned as the push–pull anisotropic ICT band because of the nature from HOMO to LUMO, HOMO to LUMO + 1, HOMO – 1 to LUMO, and HOMO – 1 to LUMO + 1, respectively. In the SM region, there are three absorptions located at 453, 432 and 379 nm, with  $f$  values of 0.154, 0.914, and 0.268, respectively, which correspond to the promotion of an electron from the HOMO – 1 to LUMO + 4, HOMO to LUMO + 5, and HOMO – 1 to LUMO + 5, respectively. Since the HOMO – 1, HOMO, LUMO + 4 and LUMO + 5 mainly contribute from the  $B_{F1_2}$ – $D_F$ – $B_{F2_2}$  fragment, these absorptions in the SM wavelength region can therefore be defined as the  $\pi$ – $\pi^*$  absorption bands of the  $B_{F1_2}$ – $D_F$ – $B_{F2_2}$  donor fragment in **X2**. The overlapping region covering the range from 470 to 520 nm is composed of three absorptions peaking at 519, 505, and 470 nm, with  $f$  values of 0.426, 0.240, and 0.430, respectively. The one at 519 comes from the coupling of electronic transitions of HOMO – 2 to LUMO + 2 and HOMO to LUMO + 4. The remaining two bands are mainly attributed to the transitions from HOMO – 2 to LUMO + 3, HOMO – 3 to LUMO + 2. As a consequence, these absorptions in this overlapping region actually originate from the mixing of two types of electron transitions: the ICT from the  $B_{F1_2}$ – $D_F$ – $B_{F2_2}$  donor fragment to the  $A_{F_S}$  and the  $\pi$ – $\pi^*$  transition in the  $B_{F1_2}$ – $D_F$ – $B_{F2_2}$  donor fragment itself.

### 3.2. Match between the donor and acceptor material

For practical application in solar cell devices, it is crucial to predict the match between the donor and acceptor in the form of their HOMO and LUMO positions. Generally, the LUMO of the donor must be positioned above the LUMO of the acceptor by at least 0.2–0.3 eV<sup>3,9</sup> to ensure the charge separation. For simplicity, this energy difference is denoted as  $E_d$  (Scheme 1) in this paper. The HOMO and LUMO energy levels of the donor and acceptor components should have an optimal offset to maximize the open-circuit voltage ( $V_{oc}$ , see Scheme 1).<sup>2a</sup> The predicted HOMO and LUMO energy levels for the donor and acceptor candidates investigated in this paper are compared in Fig. 6 and Table S7<sup>†</sup>, together with available experimental data. **PD11**<sup>18</sup> and **PD12**<sup>17</sup> have been previously applied to the field-effect transistor and photovoltaic devices. Here, it is worthy to note that our calculated results for the HOMO and LUMO energy levels are reasonably comparable with the available experimental results (e.g., HOMO/LUMO:  $-6.81/-4.02$  eV vs.  $-6.04/-4.07$  eV<sup>18</sup> for **PD12**). The  $E_d$  values between the two designed donors and the two acceptors (**PD11** and **PD12**) are in the range of 0.34–0.39 eV, assuring that both **PD11** and **PD12** are available acceptor materials *versus* the two designed donor molecules, though their LUMOs can still be improved towards the threshold  $E_d$  values.

With the aim to further enhance the match between the acceptors and the two designed donors, a series of alternative acceptor candidates are constructed by replacing substituents on the diimide N atoms in **PD11** or **PD12** by different alkyl substituents (Scheme 2). As expected, the HOMO and LUMO energy levels vary with the size of the substituents. For derivatives with the same type of substituents, the HOMOs and LUMOs increase with an increase in the number of carbon atoms

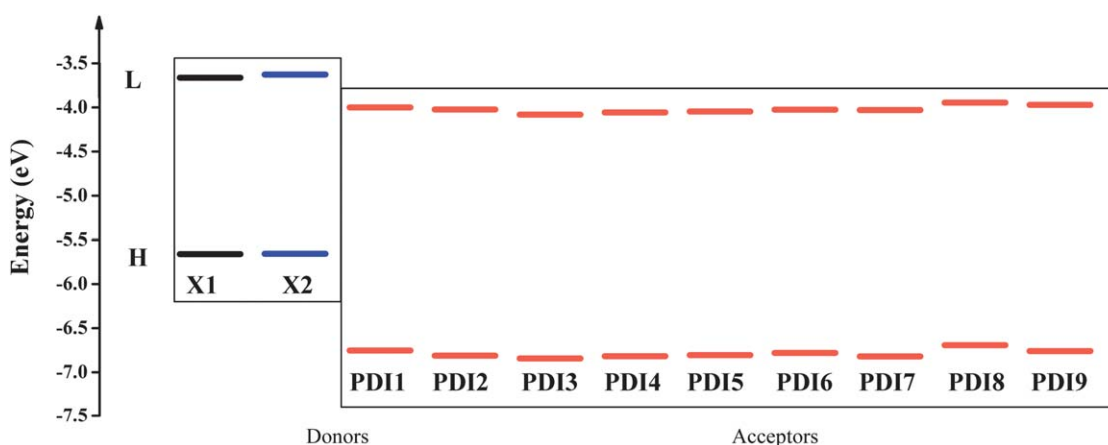


**Fig. 6** Molecular orbital energy level diagrams of two designed donors and the potential acceptors at the PBE0/6-31G(d) level (H = HOMO, L = LUMO).

(PDI3 < PDI4 < PDI5; PDI6 < PDI9); for derivatives with branched-alkyl substituents possessing the same total number of carbon atoms, the larger number of the branches results in the higher FMO energies (PDI5 < PDI6 and PDI7 < PDI8). These results suggest that longer and more branched alkyl (bulkier) substituents can cooperatively result in enhanced FMO energies.

All seven investigated PDIs acceptor candidates have proper HOMOs which are lower than those of X1 and X2 by more than 1.0 eV. Meanwhile, the differences between the HOMOs of X1 and X2 and the LUMOs of PDI8 and PDI9 (1.68–1.72 eV) are larger than those between the HOMOs of X1 and X2 and LUMOs of the other PDIs (1.57–1.63 eV). These energy differences within the range of 1.68–1.72 eV are large enough to provide high  $V_{oc}$  for organic solar cells. Furthermore, the two acceptor candidates (PDI8 and PDI9) have ideal LUMOs (−3.94 and −3.97 eV) whose deviation with those of the donor are in the range from 0.28 to 0.34 eV. On the other hand, for PDI8, the maximum absorption wavelength was obtained at 514 nm, which agrees well with the available experimental result (522 nm<sup>17</sup>), and that for PDI9 was predicted at 509 nm. (Table S4†) More importantly, the absorption spectra of the donors and PDI8 nicely complement in the visible range of the solar spectrum (Fig. 3), which in turn could further enhance the overlap of the absorption of the active layer with the solar spectrum. This further indicates that blending X1 or X2 with PDI8 may help in generating a higher photocurrent in photovoltaic devices by absorbing more sunlight. Thus, on the basis of electronic and optical consideration, PDI8 appears to be the most promising candidate as an acceptor *versus* two designed donors. For the sake of device morphology,<sup>48,49</sup> PDI9 which has bulkier alkyl substituents, could be preferred for the use as an active component in the bulk heterojunction (BHJ) solar cells in conjugation with the two designed donor materials.

### 3.3. Reorganization energies

The charge carrier mobility for the hole and electron and their balance are key parameters for efficient photovoltaic devices.<sup>48–51</sup> Generally, the lower the reorganization energy  $\lambda$  values, the better the charge carrier mobilities. For X1, X2, PDI8, and PDI9,

the calculated results predict lower  $\lambda_h$  values (in the range of 0.114–0.175 eV) than that of *N,N'*-diphenyl-*N,N*-bis(3-methylphenyl)-(1,1'-biphenyl)-4,4'-diamine (TPD, 0.290 eV)<sup>52</sup> which is a typical hole transport material, and lower  $\lambda_e$  values (in the range of 0.056–0.263 eV) in comparison with that for tri(8-hydroxyquinolato)aluminum(III) (Alq3, 0.276 eV)<sup>53</sup> which is a classical electron transport material (see Table S8†). Accordingly, our results demonstrate that the two designed donors possess good intrinsic charge carrier mobilities. Such an observation confirms our prediction that high charge mobility may be achieved for the target molecules by the combination of various building blocks with excellent charge transporting properties. Furthermore, the calculated low reorganization energies for PDI8 and PDI9 are consistent with the good electron mobility observed for the PDIs.<sup>17,18</sup> The magnitudes of  $\lambda_h$  and  $\lambda_e$  are quite close for X1, X2, PDI8, and PDI9. Considering only the activation energies for electron hopping, our data imply that all of the components have good charge transfer balance properties.

The fact that the two designed molecules have low  $\lambda_h$  and  $\lambda_e$  values can be rationalized upon careful examination of the geometric changes from the optimized neutral structures to the optimized cationic/anionic structures. The two designed molecules remain planar and only the C–N, C–C, N–S, and C–S bond distances have minor changes (within 0.017 Å for both X1 and X2, see Fig. 7) in different charge states. These small bond length changes indicate that the two designed molecules have good geometrical-adjustment ability. The relative geometry changes between the cationic and neutral state occur mainly on the central B<sub>F</sub>1<sub>2</sub>–D<sub>F</sub>–B<sub>F</sub>2 fragment, while the geometry changes between the anionic and the neutral state focus almost only on the A<sub>F</sub>S (Fig. 7). Therefore, the origin of such geometric relaxation character is believed to be the behavior of the novel (A<sub>F</sub>–B<sub>F</sub>1)<sub>2</sub>–D<sub>F</sub>–(B<sub>F</sub>2–A<sub>F</sub>)<sub>2</sub> constituents, which is the key factor for the low reorganization energies for the two designed molecules.

### 3.4. Stabilities

The molecular electronic potentials (MEP)<sup>43,54–57</sup> are also studied to evaluate the stability of the designed donor molecules, which is

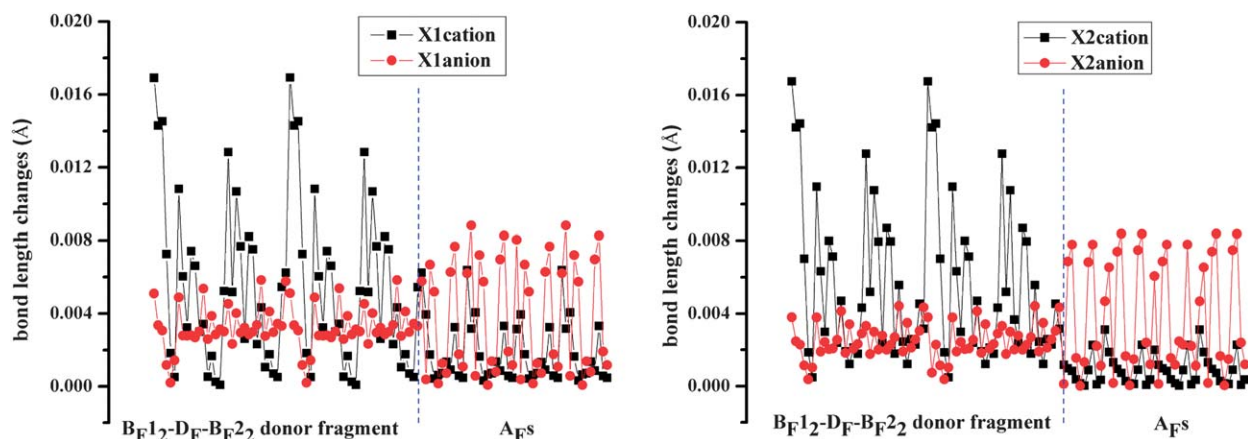


**Fig. 7** Absolute values of the bond length differences between the neutral and ionic states for X1 (left) and X2 (right). Each figure is divided into two parts by the blue dash line.

one of the key material parameters for the practical application in organic solar cells.<sup>48,58</sup> In Fig. S4†, the MEP pattern for X1 is similar to that of X2, and the slight difference is observed on the S atoms in the thiophene rings, which are adjacent to the A<sub>F</sub>s. Slightly more positive charges are displayed on the S atoms of X1 with respect to X2, indicating that X2 may be slightly more stable than X1.

#### 4. Conclusions

We have proposed a simple strategy, using double overlapping wave bands for broad and intensive absorption, to design novel high performance donor molecules for solar cells based on three types of high mobility building blocks, *i.e.*, the multibranching D<sub>F</sub>, the different B<sub>F</sub>, and the proper A<sub>F</sub>. The multibranching π-conjugated D<sub>F</sub>-(B<sub>F</sub>)<sub>n</sub> donor fragment provides the strong and broad SM π-π\* absorption, while the anisotropic multibranching ICT between the D<sub>F</sub>-(B<sub>F</sub>)<sub>n</sub> donor fragment and A<sub>F</sub>s favours for strong and broad ML absorption. With the theoretical design of the planar X-shaped (A<sub>F</sub>-B<sub>F</sub>)<sub>2</sub>-D<sub>F</sub>-(B<sub>F</sub>)<sub>2</sub>-A<sub>F</sub>)<sub>2</sub> conjugated donor molecules (X1 and X2), bearing BDT as D<sub>F</sub>, bithiophene (B<sub>F</sub>1) and ethynyl-bithiophene (B<sub>F</sub>2) as anisotropic multiple B<sub>F</sub>s, and CN substituted thiadiazolo[3,4-c]pyridine (A<sub>F</sub>1 or A<sub>F</sub>2) as the strong A<sub>F</sub>s, *versus* proper PDIs, PDI8 and/or PDI9, as the acceptor material, this concept is well established. The DFT and TD-DFT calculations demonstrated that both donors exhibit strong and broad absorption, high charge carrier mobilities, and possess narrow energy gaps as well as appropriate FMO energy levels *versus* specific acceptors, PDIs, making them promising candidates for photovoltaic applications. In addition, to form the different domains for donor and acceptor molecules in the BHJ solar cells effectively, PDI9 may be preferred as the acceptor candidates toward the two designed donor molecules.

#### Acknowledgements

This work is supported by the National Natural Science Foundation of China (50873020), JLSDF (20082212), and the Fundamental Research Funds for the Central Universities. The authors also thank Dr Josphert N. Kimatu for assisting in the proof-reading this manuscript.

#### Notes and references

- 1 J. Roncali, *Acc. Chem. Res.*, 2009, **42**, 1719.
- 2 L. Schmidt-Mende, A. Fechtenkotter, K. Mullen, E. Moons, R. H. Friend and J. D. MacKenzie, *Science*, 2001, **293**, 1119.
- 3 M. C. Scharber, D. Mühlbacher, M. Koppe, P. Denk, C. Waldauf, A. J. Heeger and C. J. Brabec, *Adv. Mater.*, 2006, **18**, 789.
- 4 Y.-J. Cheng, S.-H. Yang and C.-S. Hsu, *Chem. Rev.*, 2009, **109**, 5868.
- 5 H.-Y. Chen, J. Hou, S. Zhang, Y. Liang, G. Yang, Y. Yang, L. Yu, Y. Wu and G. Li, *Nat. Photonics*, 2009, **3**, 649.
- 6 Y. Zou, A. Najari, P. Berrouard, S. Beaupré, B. Réda Aïch, Y. Tao and M. Leclerc, *J. Am. Chem. Soc.*, 2010, **132**, 5330.
- 7 H. K. Tian, J. W. Shi, D. H. Yan, L. X. Wang, Y. H. Geng and F. S. Wang, *Adv. Mater.*, 2006, **18**, 2149.
- 8 T. Michinobu, K. Okoshi, H. Osako, H. Kumazawa and K. Shigehara, *Polymer*, 2008, **49**, 192.
- 9 N. Blouin, A. Michaud, D. Gendron, S. Wakim, E. Blair, R. Neagu-Plesu, M. Belletete, G. Durocher, Y. Tao and M. Leclerc, *J. Am. Chem. Soc.*, 2008, **130**, 732.
- 10 K. M. Omer, S.-Y. Ku, Y.-C. Chen, K.-T. Wong and A. J. Bard, *J. Am. Chem. Soc.*, 2010, **132**, 10944.
- 11 G. Qian, Z. Zhong, M. Luo, D. Yu, Z. Zhang, Z. Y. Wang and D. Ma, *Adv. Mater.*, 2009, **21**, 111.
- 12 M. E. Kose, W. J. Mitchell, N. Kopidakis, C. H. Chang, S. E. Shaheen, K. Kim and G. Rumbles, *J. Am. Chem. Soc.*, 2007, **129**, 14257.
- 13 W. Zhang, S. C. Tse, J. Lu, Y. Tao and M. S. Wong, *J. Mater. Chem.*, 2010, **20**, 2182.
- 14 Y. Li and Y. Zou, *Adv. Mater.*, 2008, **20**, 2952.
- 15 W. Cui, Y. Zhao, H. Tian, Z. Xie, Y. Geng and F. Wang, *Macromolecules*, 2009, **42**, 8021.
- 16 S. Shoaee, T. M. Clarke, C. Huang, S. Barlow, S. R. Marder, M. Heeney, I. McCulloch and J. R. Durrant, *J. Am. Chem. Soc.*, 2010, **132**, 12919.
- 17 B. A. Jones, A. Facchetti, M. R. Wasielewski and T. J. Marks, *Adv. Funct. Mater.*, 2008, **18**, 1329.
- 18 W. S. Shin, H.-H. Jeong, M.-K. Kim, S.-H. Jin, M.-R. Kim, J.-K. Lee, J. W. Lee and Y.-S. Gal, *J. Mater. Chem.*, 2006, **16**, 384.
- 19 G. D. Sharma, P. Suresh, J. A. Mikroyannidis and M. M. Stylianakis, *J. Mater. Chem.*, 2010, **20**, 561.
- 20 S. Tang and J. Zhang, *Int. J. Quantum Chem.*, 2010, **111**, 2089.
- 21 U. Salzner, *J. Phys. Chem. A*, 2010, **114**, 5397.
- 22 Sanjio S. Zade, N. Zamoshchik and M. Bendikov, *Chem.-Eur. J.*, 2009, **15**, 8613.
- 23 B. Hu and J. Zhang, *Polymer*, 2009, **50**, 6172.
- 24 S. Muhammad, H. Xu, M. R. S. A. Janjua, Z. Su and M. Nadeem, *Phys. Chem. Chem. Phys.*, 2010, **12**, 4791.
- 25 M. A. De Oliveira, H. A. Duarte, J.-M. Pernaut and W. B. De Almeida, *J. Phys. Chem. A*, 2000, **104**, 8256.
- 26 C. Adamo and V. Barone, *J. Chem. Phys.*, 1999, **110**, 6158.
- 27 M. Ernzerhof and G. E. Scuseria, *J. Chem. Phys.*, 1999, **110**, 5029.

- 28 G. Gahungu and J. Zhang, *Phys. Chem. Chem. Phys.*, 2008, **10**, 1743.
- 29 G. Gahungu, B. Zhang and J. Zhang, *J. Phys. Chem. C*, 2007, **111**, 4838.
- 30 D. Jacquemin and E. A. Perpète, *Chem. Phys. Lett.*, 2006, **429**, 147.
- 31 D. Jacquemin, J. Preat, V. Wathelet, M. Fontaine and E. A. Perpète, *J. Am. Chem. Soc.*, 2006, **128**, 2072.
- 32 E. A. Perpète, J. Preat, J.-M. André and D. Jacquemin, *J. Phys. Chem. A*, 2006, **110**, 5629.
- 33 E. I. López-Martínez, L. M. Rodríguez-Valdez, N. Flores-Holguín, A. Márquez-Lucero and D. Glossman-Mitnik, *J. Comput. Chem.*, 2009, **30**, 1027.
- 34 A. D. Becke, *Phys. Rev. A: At., Mol., Opt. Phys.*, 1988, **38**, 3098.
- 35 C. Lee, W. Yang and R. G. Parr, *Phys. Rev. B*, 1988, **37**, 785.
- 36 P. J. Stephens, F. J. Devlin, C. F. Chabalowski and M. J. Frisch, *J. Phys. Chem.*, 1994, **98**, 11623.
- 37 A. D. Becke, *J. Chem. Phys.*, 1993, **98**, 5648.
- 38 K. Takimiya, Y. Konda, H. Ebata, N. Niihara and T. Otsubo, *J. Org. Chem.*, 2005, **70**, 10569.
- 39 H. Pan, Y. Li, Y. Wu, P. Liu, B. S. Ong, S. Zhu and G. Xu, *Chem. Mater.*, 2006, **18**, 3237.
- 40 Y.-C. Hung, J.-C. Jiang, C.-Y. Chao, W.-F. Su and S.-T. Lin, *J. Phys. Chem. B*, 2009, **113**, 8268.
- 41 M. J. Frisch, G. W. Trucks, H. B. Schlegel, G. E. Scuseria, M. A. Robb, J. R. Cheeseman, G. Scalmani, V. Barone, B. Mennucci, G. A. Petersson, H. Nakatsuji, M. Caricato, X. Li, H. P. Hratchian, A. F. Izmaylov, J. Bloino, G. Zheng, J. L. Sonnenberg, M. Hada, M. Ehara, K. Toyota, R. Fukuda, J. Hasegawa, M. Ishida, T. Nakajima, Y. Honda, O. Kitao, H. Nakai, T. Vreven, J. A. Montgomery, Jr., J. E. Peralta, F. Ogliaro, M. Bearpark, J. J. Heyd, E. Brothers, K. N. Kudin, V. N. Staroverov, R. Kobayashi, J. Normand, K. Raghavachari, A. Rendell, J. C. Burant, S. S. Iyengar, J. Tomasi, M. Cossi, N. Rega, J. M. Millam, M. Klene, J. E. Knox, J. B. Cross, V. Bakken, C. Adamo, J. Jaramillo, R. Gomperts, R. E. Stratmann, O. Yazyev, A. J. Austin, R. Cammi, C. Pomelli, J. W. Ochterski, R. L. Martin, K. Morokuma, V. G. Zakrzewski, G. A. Voth, P. Salvador, J. J. Dannenberg, S. Dapprich, A. D. Daniels, J. B. ÖFarkasForesman, J. V. Ortiz, J. Cioslowski, and D. J. Fox, *Gaussian 09*, Gaussian, Inc., Wallingford CT, 2009.
- 42 R. A. Marcus, *J. Chem. Phys.*, 1956, **24**, 966.
- 43 J. E. Norton and J.-L. Brédas, *J. Am. Chem. Soc.*, 2008, **130**, 12377.
- 44 M. C. R. Delgado, E.-G. Kim, D. t. A. d. S. Filho and J.-L. Bredas, *J. Am. Chem. Soc.*, 2010, **132**, 3375.
- 45 G. N. Vayssilov, J. A. Lercher and N. Rosch, *J. Phys. Chem. B*, 2000, **104**, 8614.
- 46 D. E. Elmore, *J. Am. Chem. Soc.*, 2007, **129**, 14527.
- 47 H. Zhou, L. Yang, S. C. Price, K. J. Knight and W. You, *Angew. Chem., Int. Ed.*, 2010, **49**, 7992.
- 48 J. Peet, A. J. Heeger and G. C. Bazan, *Acc. Chem. Res.*, 2009, **42**, 1700.
- 49 D. Venkataraman, S. Yurt, B. H. Venkatraman and N. Gavvalapalli, *J. Phys. Chem. Lett.*, 2010, **1**, 947.
- 50 J.-L. Bredas and J. R. Durrant, *Acc. Chem. Res.*, 2009, **42**, 1689.
- 51 B. Kippelen and J. L. Bredas, *Energy Environ. Sci.*, 2009, **2**, 251–261.
- 52 N. E. Gruhn, D. A. da Silva Filho, T. G. Bill, M. Malagoli, V. Coropceanu, A. Kahn and J.-L. Bredas, *J. Am. Chem. Soc.*, 2002, **124**, 7918.
- 53 B. C. Lin, C. P. Cheng, Z.-Q. You and C.-P. Hsu, *J. Am. Chem. Soc.*, 2005, **127**, 66.
- 54 G. Y. Yang, M. Hanack, Y. W. Lee, Y. Chen, M. K. Y. Lee and D. Dini, *Chem.–Eur. J.*, 2003, **9**, 2758.
- 55 M. C. R. Delgado, K. R. Pigg, D. t. A. da Silva Filho, N. E. Gruhn, Y. Sakamoto, T. Suzuki, R. M. Osuna, J. Casado, V. c. Hernández, J. T. L. p. Navarrete, N. G. Martinelli, J. Cornil, R. S. Sánchez-Carrera, V. Coropceanu and J.-L. Brédas, *J. Am. Chem. Soc.*, 2009, **131**, 1502.
- 56 B. Hu, J. Zhang and Y. Chen, *Eur. Polym. J.*, 2011, **47**, 208.
- 57 A. Irfan and J. Zhang, *Theor. Chem. Acc.*, 2009, **124**, 339.
- 58 J. L. Delgado, P.-A. Bouit, S. Filippone and N. Martin, *Chem. Commun.*, 2010, **46**, 4853.